*Manuscript
Click here to view linked References

GEAR TRANSMISSION DYNAMIC: EFFECTS OF TOOTH PROFILE DEVIATIONS AND SUPPORT FLEXIBILITY

A. Fernández, M. Iglesias, A. de-Juan, P. García, R. Sancibrián, F. Viadero*

Department of Structural and Mechanical Engineering, University of Cantabria. Avda. de los Castros s/n 39005 Santander, Spain.

Corresponding Author *
Tel +34 (942) 20 18 54
Fax +34 (942) 20 18 53
viaderof@unican.es

ABSTRACT

In this work a non-linear dynamic model of spur gear transmissions previously developed by the authors is extended to include both desired (relief) and undesired (manufacture errors) deviations in the tooth profile. The model uses a hybrid method for the calculation of meshing forces, which combines *FE* analysis and analytical formulation, so that it enables a very straightforward implementation of the tooth profile deviations. The model approach handles well non-linearity due to the variable meshing stiffness and the clearances involved in gear dynamics, also including the same phenomena linked to bearings. In order to assess the ability of the model to simulate the impact of the deviations on the transmission dynamics, an example is presented including profile deviations under different values of transmitted torque. Several results of this example implementation are presented, showing the model's effectiveness.

KEYWORDS

Gear Dynamics, Bearings, Tip Relief, Profile Errors, Meshing Stiffness

1. INTRODUCTION

Today, gear transmissions are under great pressure to improve their performance, in terms of levels of power, speed, efficiency and compactness. A significant increase in the operating speeds is expected in the medium and long term, and consequently dynamic phenomena will become more important in the future, justifying further interest in the development of more accurate dynamic models.

In gear dynamics there is a particular feature that governs the vibratory behaviour, namely the presence of a parametric excitation as a consequence of the changes in the number of teeth pairs contacting simultaneously. This aspect makes the development of dynamic models cumbersome, because a balance must be achieved between accuracy and computational time [1]. Moreover, due to the non-linearity inherent to contact problems, as well as to clearances and deflections of teeth and supports, the amplitude of the torque also affects the meshing stiffness.

Bearings and gears present a similar behaviour, in the sense that bearings also undergo a parametric excitation, in this case due not only to the changes in the number of rolling

elements supporting the transmitted load, but also because of the non-linearity related to clearances and surface contacts.

Therefore, gear transmissions should be considered as a whole, including the dynamic effects of gear and bearings, particularly if a better understanding of the transmission behaviour is required for condition monitoring purposes. With this objective, in previous works the authors presented a numerical model which combined gears and bearings, with the capability of representing all the features described above. In [2] the authors described the model for calculation of meshing and bearing forces, carrying out several quasi-static analyses to show the differences in gear centre orbits, transmission error and meshing stiffness values for several transmitted torques. Subsequently, in [3] the procedure used for gear force calculation, based on a hybrid approach combining numerical and analytical tools, was extended including dissipative forces due to friction and squeeze damping. The model was assessed in dynamic simulations, speeding up the computation time by using a pre-calculated value for the meshing stiffness. Later, in [4] the dynamic model was linearized for several torque levels, obtaining the natural frequencies and mode shapes which are essential to understand the vibratory behaviour of the transmission. Moreover, gear defects such as pitting and cracks were also included, carrying out quasi-static analysis to assess the consequences [5].

Another important kind of deviations should be taken into account when modelling gear transmissions. Although the theoretical form of the profile of the flank of a spur gear is an involute, in practice it is not possible to make perfect profiles, so the real flanks present deviations from the ideal shape. These errors are directly related to the level of noise transmission produced, and have been considered by different authors. Kahraman [6] classified them as an internal source of excitation which, combined with pitch errors, teeth and supports deflections, gives the so-called transmission error. This error is defined as the difference between the actual angular position of the driven gear and the theoretical position where it would be if the gears were perfectly shaped and infinitely rigid. It is well known that the noise level of a transmission is strongly influenced by the manufacturing quality of the gears. This aspect has been studied by Bonori et al. [7] who developed a procedure for generating random profile errors in a range of tolerances established for all pinion and gear teeth. These individual errors were combined for a complete transmission cycle and expanded in a Fourier series for its implementation in a dynamic model. From the simulation results, the authors concluded that the inclusion of these errors leads to a significant increase in the vibration amplitude throughout the whole frequency range. They also pointed out that this increase is most apparent at low speeds and torque loads, where non linearity related with contact loss can appear more easily. This fact has also been addressed specifically by Ottewill et al. [8], who concluded that even tiny tooth profile errors can have a major effect on gear rattle.

Sometimes the profile changes are desired and they are introduced in a premeditated manner. These consist in modifications of the original profile by certain relief in the near–tip area (Tip relief) or at the base of the tooth (Bottom relief) with which a significant improvement in the noise and vibration levels is achieved. This is an aspect that has also received attention from many authors. The models that can be found in the literature addressing this kind of modification, generally consider that changes in the profiles are so small that the Line of Action (*LOA*) of the contact forces does not

change, in such a way that there is only a reduction in the magnitude of the geometric overlap between the profiles of the teeth in contact, in comparison with the non-modified case [1], [9].

In this work, profile deviations such as tip reliefs and undesired profile errors are added to the dynamic model previously developed by the authors, with the aim of analysing the consequences on the dynamic behaviour under several torque loads. As a consequence of the supports flexibility, the amplitude of the transmitted torque modifies the distance between centres and the pressure angle, producing an alteration of the conditions of contact between gears. In addition, due to teeth deformations, both the effective contact ratio and the meshing stiffness are modified. The model presented enables the consideration of these phenomena due to the formulation of the local contact (which is non-linear). Furthermore, the model also takes into account the consequences of teeth deflection as well as the possible changes in the distance between gear centres. This aspect becomes particularly interesting to improve the design procedure to determine the parameters which define the profile relief.

2. DESCRIPTION OF THE MODEL

In this section the proposed model is briefly explained, paying greater attention to the formulation used to include profile deviations. More details about the model can be found in references [2], [3], [4] and [5].

Gear forces are obtained following the proposal of Vedmar and Andersson [10] in which the deformation at each gear contact point is formulated as a combination of a global (or structural) term obtained by means of a *FE* model, and a local term described by an analytical approach which derives from Hertzian contact theory.

The tooth profile geometry necessary to build the *FE* model is generated using a rack-type tool following Litvin's vector approach [11]. For the *FE* model it is assumed that the nodes in the inner circle are fixed, that is, where the gears are fitted to the shaft. Multiple load cases are considered, each of which is defined by a unit load perpendicular to the tooth profile located at different radial positions from the root to the tip. Then the *FE* model built for each gear is solved once, before the integration of dynamic equations, obtaining the displacement (flexibility) of the node *j* due to a unitary load applied in the node *i* of the loaded active flank. These flexibilities are used to solve the contact problem imposing the compatibility of geometrical separations (δ_j) and elastic deflections (u_{Tj}) submitted to the complementary condition (in order to avoid non-realistic negative loads) arriving at the following non-linear system of equations for *n* contacting points

$$\begin{aligned} &\delta_j(\{\vec{r}_p,\theta_p\},\{\vec{r}_w,\theta_w\}) = u_{Tj}(\{\vec{r}_p,\theta_p\}\{\vec{r}_w,\theta_w\}\{F\}) \\ &\textit{submitted to} \quad F_i \geq 0; \quad i,j = 1,...,n \end{aligned} \tag{1}$$

where $\{F\}$ is the unknown vector, which contains the contact forces F_i for each active contacting point. Subscripts *p* and *w* refers to the pinion and wheel respectively, while *r* and θ represent the centre and angular position of the gears. Meshing forces are extended including Coulomb friction with a smoothed function to avoid the singularity

corresponding to the pitch point contact. Furthermore, meshing damping is formulated as a function of the squeeze film (see [3]).

The elastic deflections (u_{Tj}) in (1) are obtained by addition of the global and local terms for both gears. At the same time, geometrical separations are obtained taking advantage of the analytical properties of involute profiles and rounding arcs (which are introduced at the tooth tip to handle the possibility of corner contacts). Therefore, two different types of contact are considered: Involute – Involute and Involute – Tip rounding contact. In the first case, the normal contact force is parallel to the *LOA* whereas for the second scenario the resultant force acts Out of the Line of Action (*OLOA*). This feature provides a smoother transition on the shape of the meshing stiffness.

As it happens with gears, the changing number of bearing rolling elements supporting the load implies a parametric excitation, function of the shaft rotational angle. This time, bearing clearance interacts with the magnitude of the load to be transmitted, defining the angular positions in which the number of rolling elements supporting the load changes. To consider these facts, bearing forces have been formulated following the model proposed by Fukata et al [12].

The presented gear and bearing formulations are implemented in a dynamic model of a single-stage transmission, which is shown in Figure 1 as a block diagram. Shaft torsional and flexural deflections are taken into account by spring-damper elements, while non-linear forces of gears and bearings are represented by two-way arrows. A reference framework is defined with *z-axis* along the shaft centre line and the *y-axis* defined by the line between gear centres. Using the subscripts *R* and *b* to designate the gears and bearings, X_{iRj} means the displacement along the *x-axis* of gear *j* of shaft *i*. The degrees of freedom (*dof*) associated with bearings and gears are grouped in vectors $\boldsymbol{q_{ibj}} = \{x_{ibj}, y_{ibj}, \theta_{ibj}\}^T$ and $\boldsymbol{q_{iRj}} = \{x_{iRj}, y_{iRj}, \theta_{iRj}\}^T$. Furthermore, an additional rotational-only inertia connected by an elastic coupling is included at the output and a constant value of rotational speed is assumed at the input.

Then, the individual element matrices (mass, damping and stiffness) are assembled into the dynamic matrix equation arriving at a system with 19 *dof*. This equation is subsequently arranged for numerical integration in *Matlab/Simulink*® arriving at

$$\begin{aligned} \ddot{\mathbf{q}} &= \mathbf{M}^{-1}\left(\mathbf{f}_{Ext}(t) - \mathbf{C}\dot{\mathbf{q}} - \mathbf{K}\mathbf{q} - \mathbf{f}_b(\mathbf{q}) - \mathbf{f}_R\left(\mathbf{q},\dot{\mathbf{q}}\right)\right) \\ \mathbf{q} &= \left\{\mathbf{q}_{1b1}, \mathbf{q}_{1R1}, \mathbf{q}_{1b2}, \mathbf{q}_{2b1}, \mathbf{q}_{2R1}, \mathbf{q}_{2b2}, \theta_{Out}\right\}^T \end{aligned} \qquad (2)$$

where **M**, **C** and **K** are constant coefficient matrices, while vectors $\mathbf{f_b}$ and $\mathbf{f_R}$ represent non-linear bearing and meshing forces. The proposed procedure allows performing dynamic simulations. Nevertheless, the need to solve the non-linear equation system (1) gives rise to long calculation times. With the aim of improving the computation speed, a previous quasi-static analysis for a meshing period was carried out, obtaining the stiffness for each contacting teeth pair as a function of the angular position. To do this, the dynamic equations in (2) were simplified neglecting the dynamic terms. The pre-calculated values obtained for the meshing stiffness are then stored in memory and used for simulations when the load and rotational speed are stationary and the system

operates far from its resonant ranges. As the stiffness is obtained for each individual contact between teeth pairs, the model structure remains unchanged and each contact is analysed individually providing a good description on the load sharing between tooth pairs.

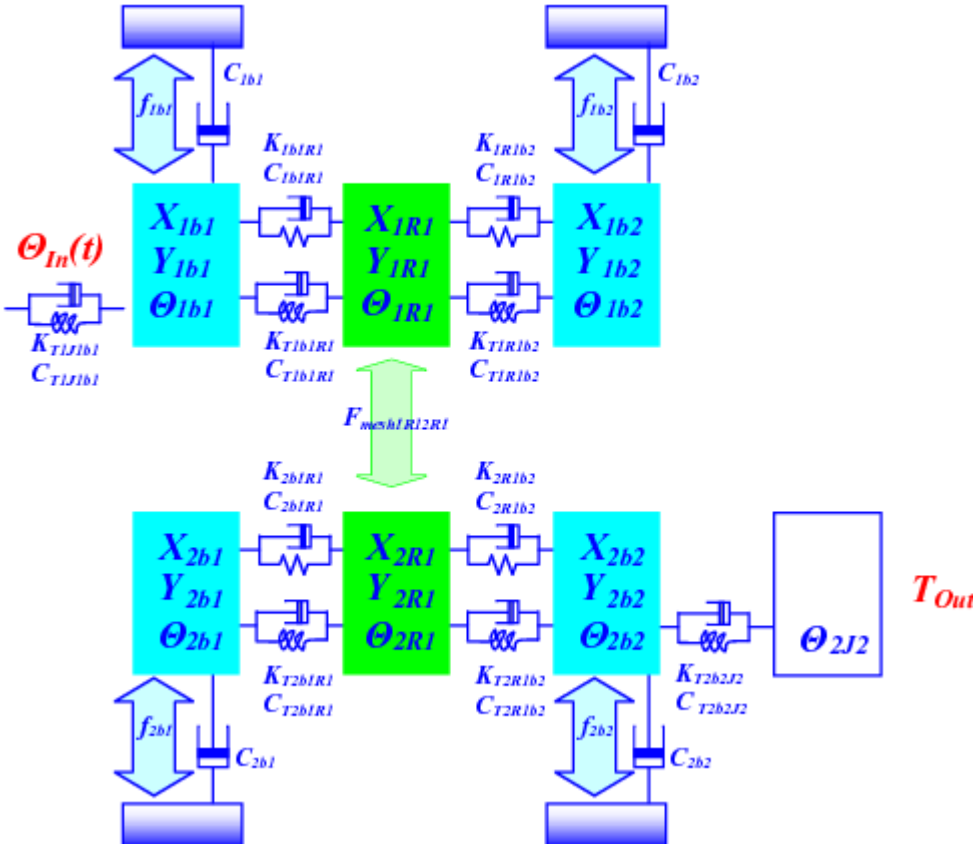

Figure 1.- Block Diagram

3. PROFILE DEVIATIONS

In order to model profile deviations, it is firstly assumed that deviations from the theoretical profile due to the manufacturing process or wear are not big enough to affect the overall flexibility of the tooth or the normal direction of the contact force. Thus, the inclusion of this phenomenon does not modify the calculation of the contact forces, and it only affects the calculation of the distance between potential contact points. This modification can be included in equation (1) obtaining

$$\delta_j(\{\vec{r}_p,\theta_p\},\{\vec{r}_w,\theta_w\}) = u_{Tj}(\{\vec{r}_p,\theta_p\}\{\vec{r}_w,\theta_w\}\{F\}) + e_{jp}\left(\{\vec{r}_p,\theta_p\}\right) + e_{jw}\left(\{\vec{r}_w,\theta_w\}\right)$$
$$\textit{submitted to} \quad F_i \geq 0; \quad i,j = 1,...,n \tag{3}$$

where e_{jp} and e_{jw} represent the pinion and wheel profile deviations corresponding to the j^{th} contacting point.

3.1. Profile Errors

In practice, being the result of the manufacturing process, Profile Errors (*PE*) errors show a similar pattern in the same flank of successive teeth. Thus, in this work *PE* are considered identical for all teeth. The formulation of such errors has been carried out following the approach proposed by Mucchi et. al. [13], adopting a sinusoidal shape with amplitude $f_{f\alpha}$ and f_r cycles as a function of the roll path length *s*, according to the expression (see

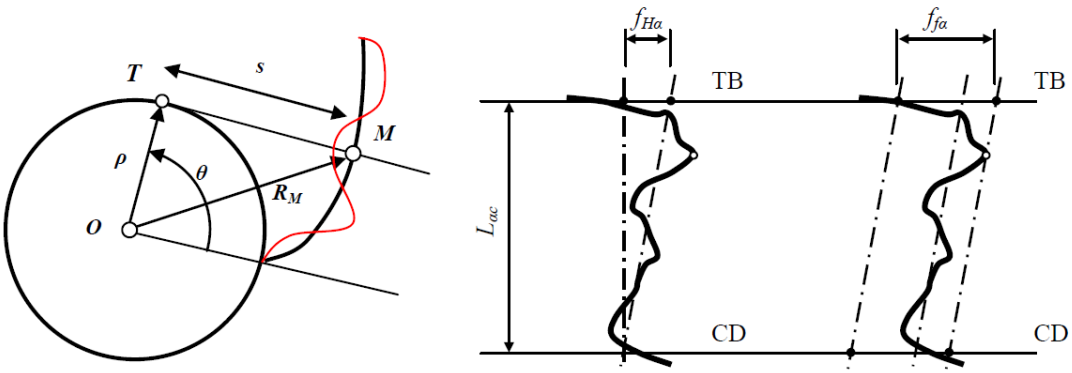

Figure 2)

$$e_{PE}(s)=f_{H\alpha}\frac{(s-s_0)}{(s_f-s_0)}+\frac{f_{f\alpha}}{2}\sin\left(2\pi f_r\frac{(s-s_0)}{(s_f-s_0)}\right) \qquad (4)$$

where $f_{f\alpha}$ is the Profile Form Deviation and $f_{H\alpha}$ the Profile Slope Deviation. Following the AGMA definition [14], the Profile Form Deviation is the "distance between two facsimiles of the mean profile line, which are each placed with constant separation from the mean profile line, so as to enclose the actual profile trace over the functional profile length" and the Profile Slope Deviation is "the distance between two design profile lines which intersect the mean profile line at the endpoints of the functional profile length".

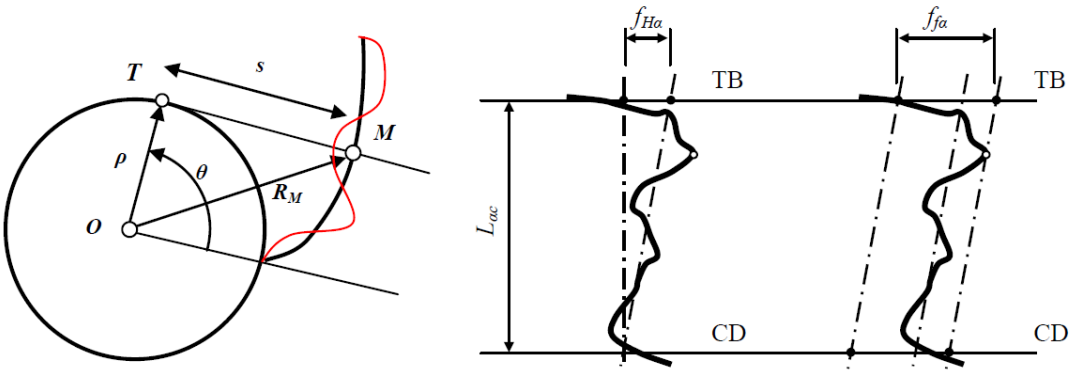

Figure 2.- Parameters defining the profile error

The functional profile length ($L_{\alpha c}$) goes from the profile control diameter *CD* (that could be the Start of the Active Profile SAP or the True involute Form TIF) to the start of the tip break *TB*. In expression (4) the profile error adopts a sinusoidal shape with amplitude $f_{f\alpha}$ and f_r cycles along the functional profile length ($L_{\alpha c} = s_f - s_0$) which is the result of the subtraction of the higher (s_f) and lower (s_0) curvature radii. Here, positive

errors mean increments of the curvature radii with respect to the nominal one, while negative values indicate reductions. This formulation could be modified as a function of the profile error shape. Once each profile error of the contacting teeth is defined, it is necessary to determine the global combined error, which is calculated by adding the errors of each of the profiles.

3.2. Profile Modifications: Tip Relief

Contrary to the undesired *PE* described in the previous section, which is a result of the manufacturing process, there are other cases in which it is necessary to include profile modifications in a deliberate manner. This is done for several purposes, such as relieving the stress level on the teeth, avoiding contact at the tip and smoothing the transmission error shape as much as possible. The introduction of changes in the profile shape at the tip (tip relief) or at the base of the tooth (bottom relief) is a common practice in the design of gears. Nevertheless, particularly in spur gears, the form and magnitude of these deviations must be carefully chosen depending on the level of torque to be transmitted. The deviations can be classified as short or long, depending on their extension, and as linear or parabolic, depending on the deviation shape. The short relief begins near the point at which the change in the number of pairs of teeth in contact occurs and it is usually employed in transmissions where the load level is low. On the contrary, if the transmission is to be subjected to high torque levels, the long relief, which can be started at the primitive point, should be employed. The short relief only affects the double contact zone while the long relief also modifies the single contact one.

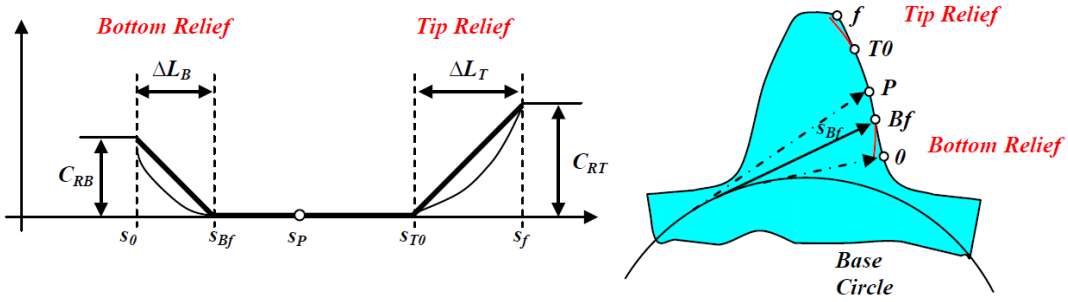

Figure 3.- Description of the tip and bottom reliefs

These profile modifications are implemented in a similar way to the *PE*. In this case, positive values of the deviation mean removal of material with respect to the nominal shape (smaller curvature radii), and negative values indicate the contrary. The formulation of this modification is defined (see

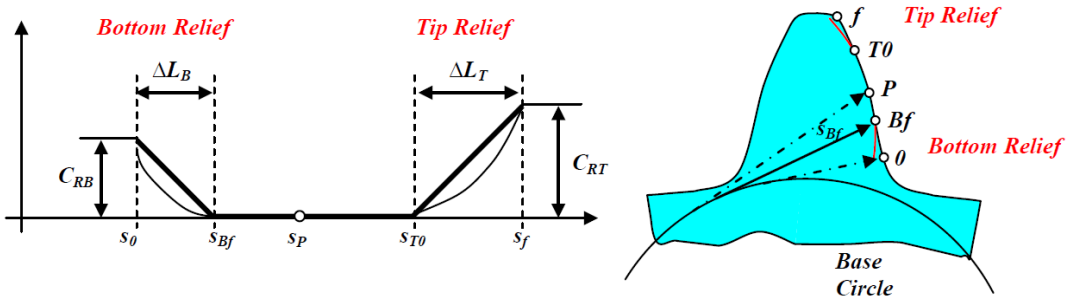

Figure 3) by the maximum magnitude of the relief (C_{RT} for the tip and C_{RB} for the bottom), the length of the correction (ΔL_B or ΔL_T) and the shape, which is generally linear or parabolic and expressed by

$$e_{RT}(s)=C_{RT}\left(\frac{(s-s_{T0})}{\Delta L_T}\right)^n \qquad n=1,2; \qquad s\in[s_{T0},s_f] \quad (5)$$

$$e_{RB}(s)=C_{RB}\left(\frac{(s_{Bf}-s)}{\Delta L_B}\right)^n \qquad n=1,2; \qquad s\in[s_0,s_{Bf}] \quad (6)$$

Where n takes the value 1 if the shape of the deviation is linear and 2 if it is parabolic.

4. APPLICATION EXAMPLE

Next, a numerical example is presented whose basic gear parameters are listed in Table 1. The pinion and wheel have the same size and are mounted in shafts which are supported by a couple of ***209*** single-row radial deep-groove ball bearings [15] described in Table 2. The gear data corresponding to the pinion have been taken from reference [16]. More details can be found in [2], [3] and [4].

Table 1.- Gear data

Parameter	***Value***	***Parameter***	***Value***
Number of teeth	28	Rack tip rounding	0.25 **m**
Module (**m**) [mm]	3.175	Gear tip rounding	0.05 **m**
Elasticity Modulus [GPa]	210	Gear face width [mm]	6.35
Poisson's ratio	0.3	Gear shaft radius [mm]	20
Pressure angle [degree]	20	Gear mass [Kg]	0.7999
Rack addendum	1.25 **m**	Gear inertia[Kgm^2]	4.0 10^{-4}
Rack dedendum	1 **m**	Oil viscosity [Pas]	0.004
Output inertia [Kg m^2]	$\boldsymbol{J_{2J2}}$= 3.56 10^{-4}	Shaft flex. Stiff. [N/m]	$\boldsymbol{K_{ib1R1}}$= $\boldsymbol{K_{iR1b2}}$ = 6.24 10^8
Shaft Tor. Stiff. [Nm/rad]	$\boldsymbol{K_{Tib1R1}}$=$\boldsymbol{K_{TiR1b2}}$=4 10^5	Coupling Stiff. [Nm/rad]	$\boldsymbol{K_{T1J1b1}}$= $\boldsymbol{K_{T2b2J2}}$=4.0 10^5
Shaft Tor. Damp. [Nms/rad]	$\boldsymbol{C_{Tib1R1}}$= $\boldsymbol{C_{TiR1b2}}$ = 0	Coupling Damp. [Nms/rad]	$\boldsymbol{C_{T1J1b1}}$= $\boldsymbol{C_{T2b2J2}}$=3.5761
Shaft Flex. Damp. [Ns/m]	$\boldsymbol{C_{ib1R1}}$= $\boldsymbol{C_{iR1b2}}$ = 31.6		

Table 2.- Bearing data

Parameter	***Value***	***Parameter***	***Value***

Contact Stiffness [N/m$^{3/2}$]	1.2 10^{10}	Ball diameter [mm]	12.7
Number of balls	9	Mass $\boldsymbol{m_{1b1}}$= $\boldsymbol{m_{2b2}}$ [Kg]	0.490
Radial clearance [μm]	15	Mass $\boldsymbol{m_{2b1}}$= $\boldsymbol{m_{1b2}}$ [Kg]	0.245
Outer race diam. [mm]	77.706	Inertia $\boldsymbol{J_{1b1}}$=$\boldsymbol{J_{2b2}}$ [Kgm^2]	9.8 10^{-5}
Inner race diam. [mm]	52.291	Inertia $\boldsymbol{J_{2b1}}$=$\boldsymbol{J_{1b2}}$ [Kgm^2]	4.9 10^{-5}
Inner groove rad. [mm]	6.6	Bearing damping 5% [Ns/m]	334.27
Outer groove rad. [mm]	6.6		

The *PE* defined in sub-section 3.1 has been included into the transmission example according to the values contained in Table 3. The profile error amplitude values have been considered taking into account some data available in the literature, particularly the K chart provided by Bonori et al. in [17], while frequency f_r has been extracted from the work of Mucchi et al. in reference [13].

Table 3.- Parameters for each flank profile error.

Parameter	***Pinion***	***Wheel***
$\boldsymbol{f_{H\alpha}}$***[mm]***	0.002	0.001
$\boldsymbol{f_{f\alpha}}$ ***[mm]***	0.003	0.003
$\boldsymbol{f_r}$	1.8	1.3
$\boldsymbol{s_f}$ ***[mm]***	22.8793	22.8793
$\boldsymbol{s_0}$ ***[mm]***	5.1260	5.1260

PE of a teeth couple in contact must be combined as the addition of the individual contributions of each tooth, obtaining the result shown in Figure 4 when the mounting distance corresponds to the nominal distance. Abscissas in Figure 4 numerically corresponds to the roll path length of gear 1, while the PE assigned to gear 2 is shown from right to left. The *PE* for the entire functional profile length of each tooth is represented by a dotted line, using solid lines for the portion of actual contact. Therefore, with this procedure the real shape of the combined *PE* depends on the working distance.

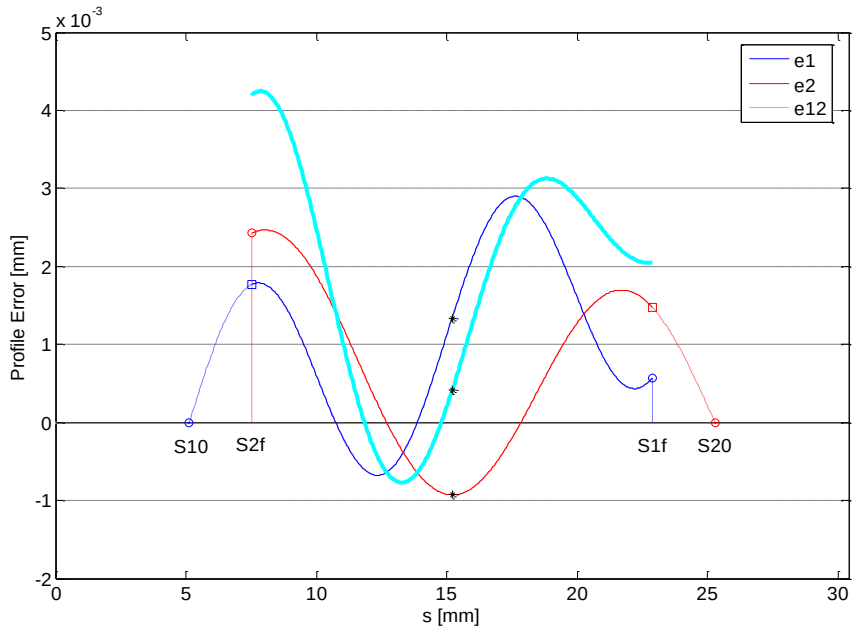

Figure 4.- Profile errors for the pinion (e_1 blue), wheel (e_2 red) and combined error (e_{12} cyan)

In order to assess the impact that the extent and magnitude of reliefs has on the behaviour of a transmission, a quasi-static analysis of the example has been carried out incorporating the linear tip reliefs described in Table 4 for both gears. Moreover, dynamic analyses were done using the case *TRL4C015* with different torque levels.

Table 4.- Tip relief parameters (see

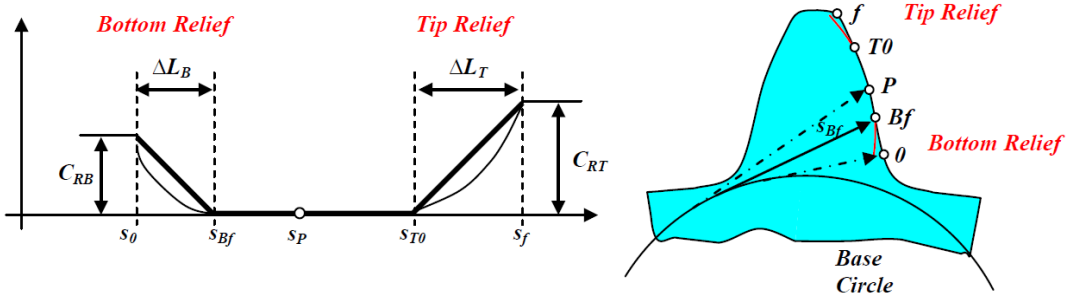

Figure 3)

$\Delta L_T \setminus C_T$	C_{RT} =0.015 mm
ΔL_T = 3 mm	TRL3C015
ΔL_T = 4 mm	TRL4C015
ΔL_T = 5 mm	TRL5C015
ΔL_T = 6 mm	TRL6C015
ΔL_T = 7 mm	TRL7C015
ΔL_T = 8 mm	TRL8C015

From the kinematic point of view the transition between single and double contact, for the gear pair analyzed, takes place at a position of 5.9800 mm measured along the *LOA* from the start of the active profile (*SAP*) while the contact at the pitch point takes place for a position of 7.6765 mm. According to these data, reliefs with lengths of 3, 4 and 5 mm can be considered short, while lengths of 6, 7 and 8 mm can be considered long.

QUASI-STATIC ANALYSIS

As a preliminary assessment of the proposed model, a quasi-static analysis was conducted by neglecting the dynamic terms in the equation (2). Then, for several angular positions of gear 1 throughout a meshing period, a torque was applied to the gear 2 and by a Newton's based numerical procedure the location of both gears centres as well as the angular position of the gear 2 (for more details about the numerical procedure see ref [18]) were calculated. From the quasi-static analysis several quantities have been obtained, such as the Loaded Transmission Error (*LTE*), the equivalent translational Meshing Stiffness, the Load Sharing Ratio (*LSR*) or the gear orbits. Special interest has been focused in the shape of the gear centre orbits which are presented in Figure 5. There, it is clear how the gear orbit is displaced along the *LOA* (around 20 deg in the example) as the torque is increased. That means changes in the centre distance as a consequence of shafts and bearing flexibility, and therefore changes in the effective pressure angle. An interesting aspect related to the orbit shape is that it is larger in the *OLOA* direction. The displacement in this direction is caused by the non-symmetric bearing stiffness with respect to the supporting direction of the load. Thus, for a constant load applied in the *LOA* the quasi-static equilibrium require *OLOA* displacements. This fact is even more evident when bearing clearance is considered. Moreover, as stated in section 2, tip rounding contacts also give place to *OLOA* forces. The *OLOA* orbit amplitude is then determined by the number of the rolling elements supporting the load as well as by how the load is shared among them (see ref. [2]). That is the reason for the load related non-linear behaviour observed in Figure 6.

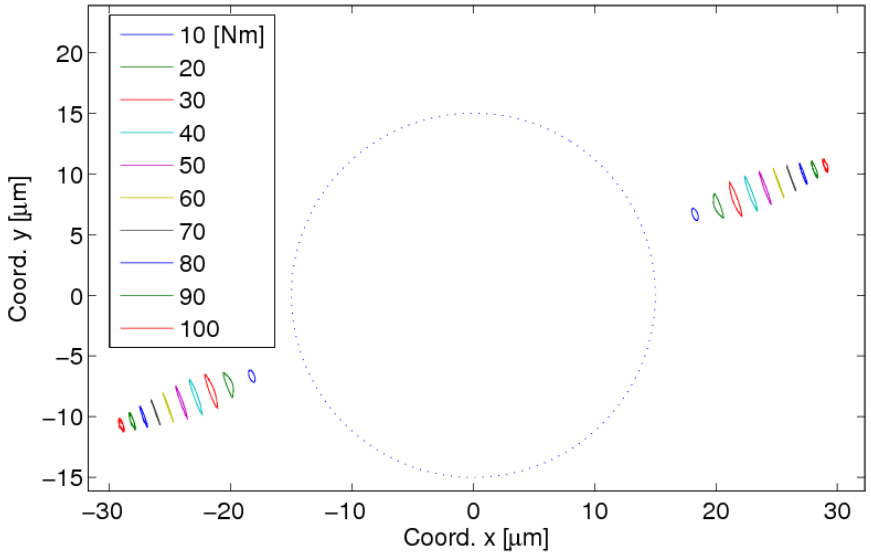

Figure 5.- Gear pair orbit for several transmitted torques. Dashed line represents the bearing clearance

During the quasi-static analysis the force and the corresponding geometrical overlap for each contact pair is obtained. As it was explained in the description of the model, this contact stiffness for each contact is stored to carry out faster dynamic simulations. As an example to show the sensitivity of this procedure to the applied torque in Figure 6 is presented the meshing stiffness for successive contact pairs thorough a meshing period considering two load cases of 10 and 100 Nm. At 0 rad the contact takes place at the

primitive point, involving only one teeth pair. That situation remains in the central region of the diagram which corresponds to the lower value of the total meshing stiffness. Then, when the torque is shared by two teeth pairs the total stiffness is increased. As the applied torque grows (up to 10 times in Figure 6 b)), the total meshing stiffness is increased only slightly. This small increment is due to the nonlinearity related with the Hertzian contact. On the other hand, due to the teeth and gear body deflection, the single contact region is narrowed and the effective contact ratio is increased even though the theoretical contact ratio should be reduced as the centre distance is increased. The combination of both phenomena gives as result an increment on the average value of the meshing stiffness which has consequences on the dynamic behaviour as the resonant frequencies are shifted to higher frequencies [4].

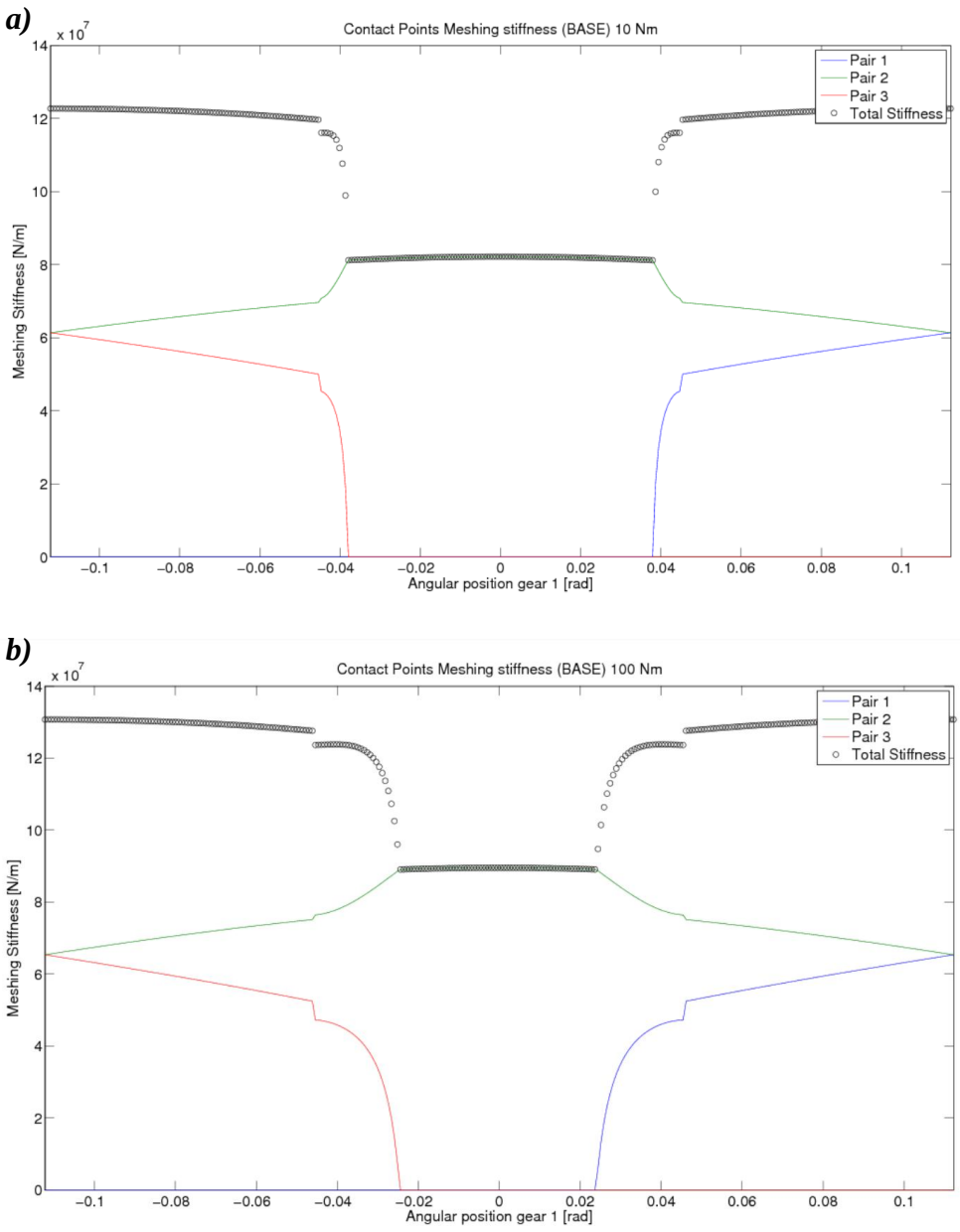

Figure 6.- Meshing Stiffness for each contact pair a) Torque 10 Nm; b) Torque 100 Nm

In order to analyze the consequences of *PE* and profile reliefs, a simple quasi-static analysis has been done taking into account only the rotational *dof* for each gear, fixing the translational displacements. In the following some results are presented.
The inclusion of *PE* completely changes the *LTE* with respect to the analysis performed with the ideal profile. In Figure 7 the results corresponding to the minimum (10 Nm) and maximum (100 Nm) applied torque are presented. When the torque level is low, the effect of the *PE* is more noticeable, while the load increments reduce the differences. In more details, the absolute contribution of the PE is comparable for the two applied torques, but it is relatively more important in the case of low torque. In both cases the transmission error is smaller because the profile error considered is basically positive so that there is a reduction of the separation distance between profiles, and thus the contact between teeth takes place earlier (even causing negative *LTE* values for low torque levels as shown in Figure 7 a).

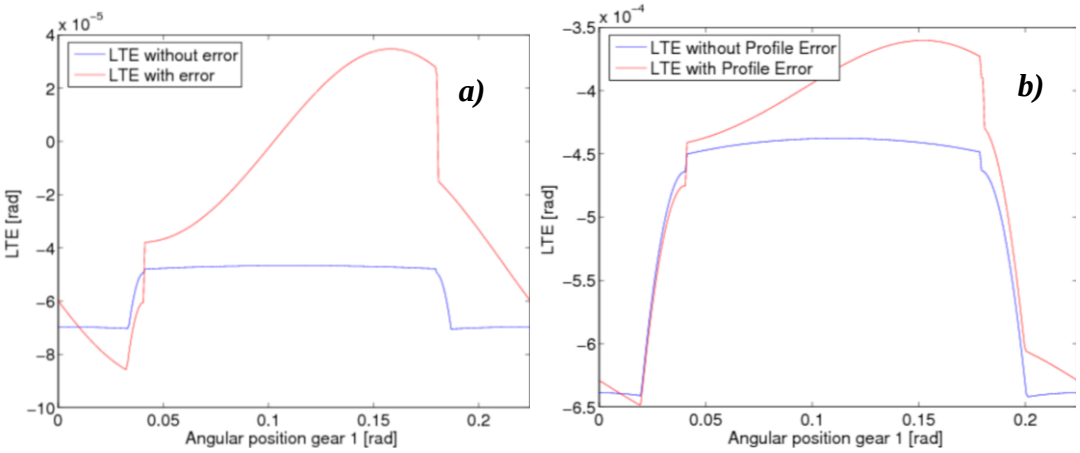

Figure 7.- *LTE* including *PE* a) 10 Nm; b) 100 Nm

Regarding tip reliefs, Figure 8 shows the resulting meshing stiffness for different lengths of tip reliefs. Except when the relief length is 3 mm, all other cases show that in the double contact area (around the central position of the figures) the meshing stiffness changes its shape from a valley to a peak when the transmitted torque increases. The value of torque which provides the smoothest transmission error (no valley or peak are presented) is called the design load. It can also be appreciated how the magnitude of the design load increases with the relief length.

It should be noticed that the meshing stiffness values for the double contact falls even below the meshing stiffness values corresponding to the single contact. This is due to the formulation of the equivalent translational meshing stiffness (K_m) used, which is derived from the *LTE* for a certain angular position of gear 1 (θ_1) under a given external torque load (T_{Ext}) by means of the equation

$$K_m(\theta_1, T_{Ext}) = \left| \frac{T_{Ext}}{\rho_2^2 LTE(\theta_1, T_{Ext})} \right| \quad (7)$$

where ρ_2 is the base radio of gear 2. When tip relief is included the double contact meshing period is reduced. This relief introduces a gap between the involute profiles which should be in contact from a kinematic point of view. This gap must be recovered by a rigid body rotation in order to achieve effective contact. Thus, the *LTE* is increased and therefore the resulting meshing stiffness (which by definition is not a real stiffness,

but an equivalent magnitude) obtained from (7) is even lower than the single contact value. The same behaviour can be observed on the results obtained by other researchers as in the work of He et al. [16]. This fact is more evident when the relief length goes below the pitch point (ΔL_T >7.6765 mm, Figure 8 case f)), where even the single contact stiffness is strongly affected and the overall stiffness is clearly lower than for the other tip relief cases, particularly for low loads.

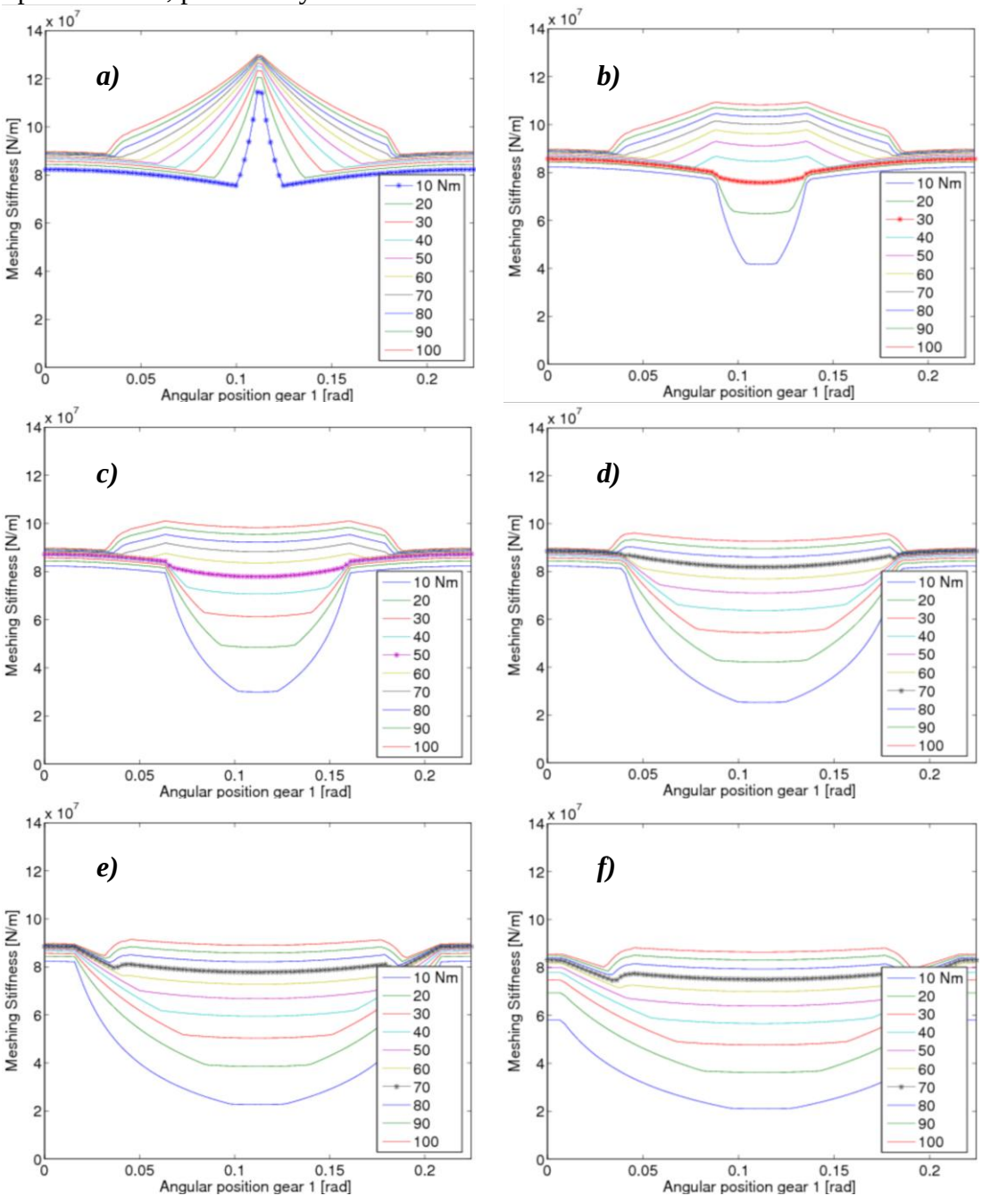

Figure 8.- Meshing Stiffness with tip relief amplitude of C_{RT} =0.015 mm and several lengths; a) ΔL_T = 3; b) ΔL_T = 4; c) ΔL_T = 5; d) ΔL_T = 6; e) ΔL_T = 7; f) ΔL_T = 8 (mm)

The selection of the parameters that define the tip relief must be done carefully, studying not only the *LTE* characteristics for the design load but also the sensitivity to

load variation and working distance. In order to assess these aspects and taking advantage of the features of the model developed, the case denominated *TRL4C015* in Table was analysed considering a load variation of about 5% around the design load, which is estimated at 32 Nm. The resulting meshing stiffness is very similar for all cases

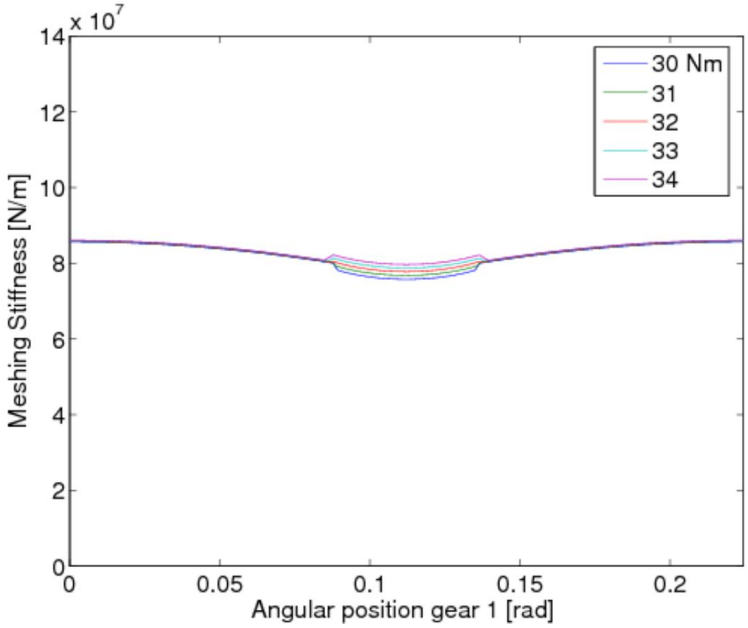

(see Figure 9). Torque values below the design load provide a valley in the double contact zone, while the higher values lead to a peak. Nevertheless, the shape in all cases appears very smooth and with low variations between the area for single and double contact. However, the spectral decomposition provides significant differences. Increments in the transmitted torque lead to a reduction in the amplitude of the first four harmonics, while higher order harmonics tend to induce a minimum value for the design load at 32 Nm. Variations in the first 3 harmonics with respect to the design load values lead to differences close to 10%, as shown in Figure 10. Therefore, when tip reliefs are included in a gear transmission, relatively small variations of the transmitted torque (around 5%) will lead to a completely different dynamic response.

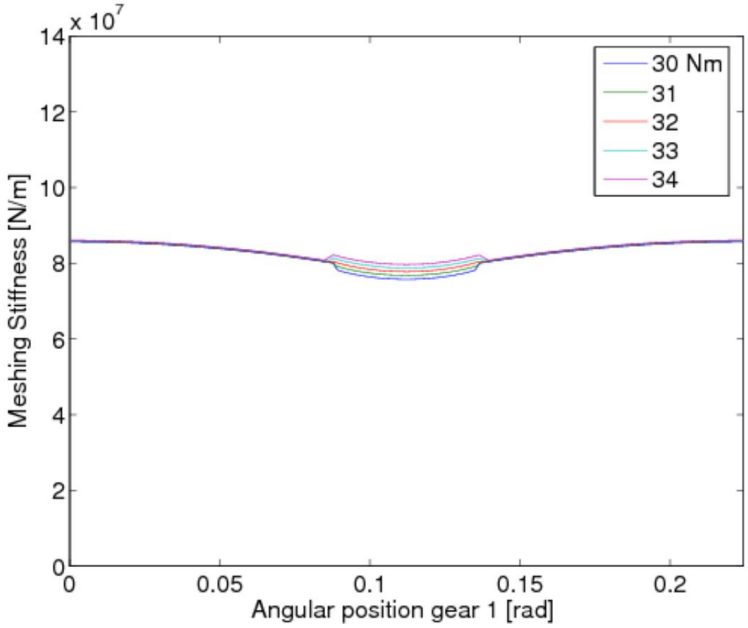

Figure 9.- Meshing stiffness variation (case *TRL4C015*) with several applied torques around the design load (32 Nm)

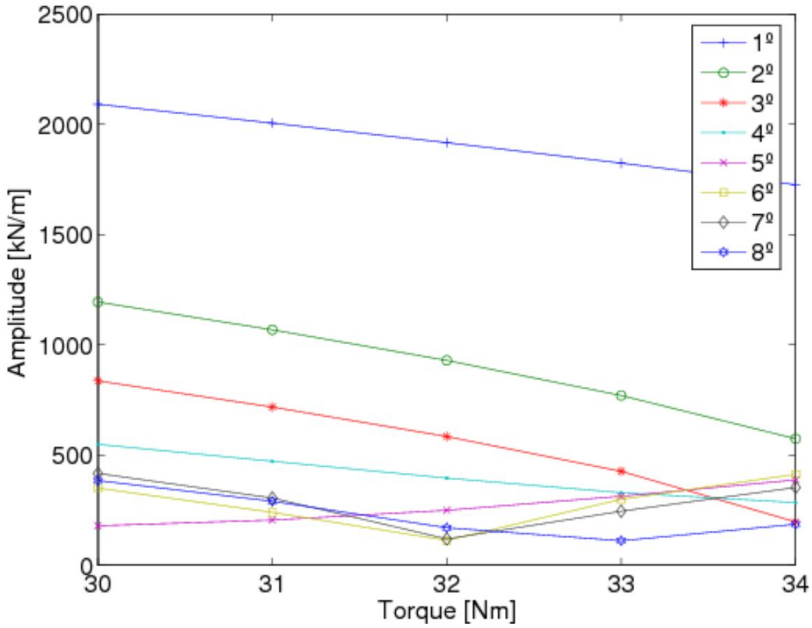

Figure 10.- Amplitude of the first 8 harmonics of Meshing Stiffness (case *TRL4C015*) when the transmitted torque varies around the design load (32 Nm)

As a result of shaft and support flexibility as well as bearing clearances, the amount of torque to be transmitted affects the effective gear centre distance. Thus, the variation of this parameter also affects the meshing stiffness, as shown in Figure 11. An increment of the working distance gives rise to a valley of increasing depths in the double contact zone. The spectral decomposition shows substantial differences again. In this case, the increased working distance brings an increase in the amplitude of almost all harmonics. Particularly significant is the increase in the magnitude of the first two harmonics, which show variations of up to 25% compared to the values corresponding to the reference mounting distance (0 mm) (see Figure 12).

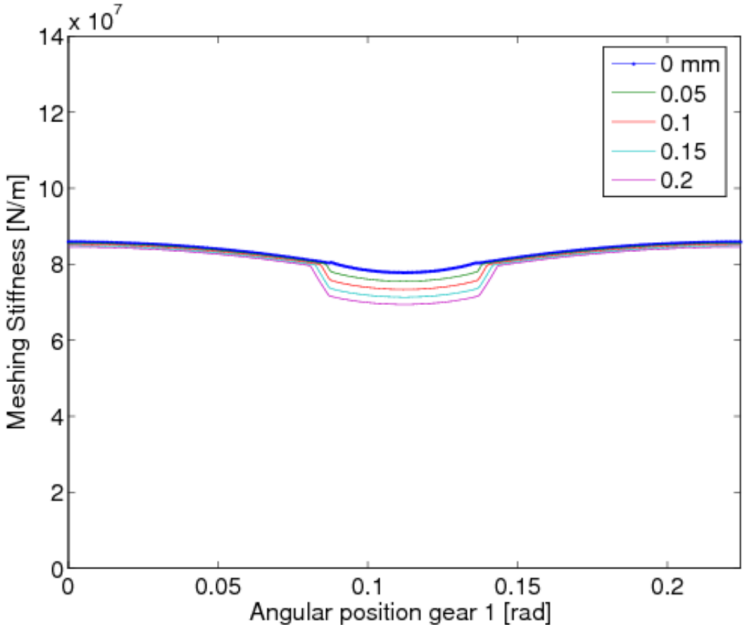

Figure 11.- Meshing Stiffness for several working distances with a transmitted torque of 32 Nm (case *TRL4C015*)

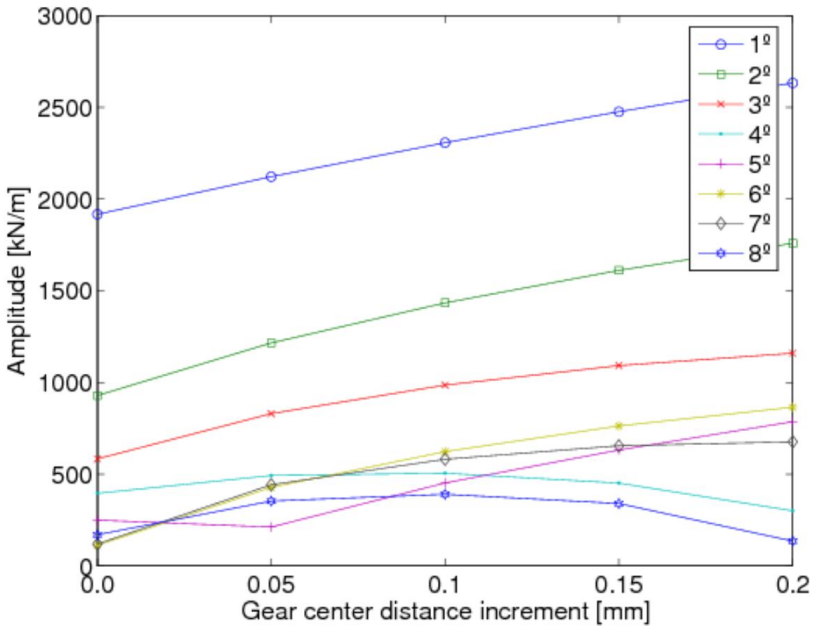

Figure 12.- Amplitude of the first 8 harmonics of Meshing Stiffness (case *TRL4C015*) with several increments on the mounting distance (32 Nm)

5. DYNAMIC ANALYSIS

In the following, some of the most noteworthy results obtained from dynamic simulations of the transmission example for a rotational speed of 1000 r.p.m. with several torque levels between 10 and 100 Nm will be presented, in order to demonstrate the model's capability. Simulations were carried out using a fixed sample frequency of 75 kHz and data output removing the transient period were recorded in a file. To reduce the transient period until the arrival of stationary conditions, the deflected position of

the bearings and gears obtained from the previous quasi-static analysis were used as initial conditions for integration. In the same way, initial rotational velocity was imposed only in the rotational DOF's.

5.1. Dynamic analysis without profile deviations

Figure 13 shows the resultant *LTE* for several torque levels without profile deviations. There, the cyclic nature due to the meshing period can be clearly identified. Moreover, for lower torque levels, it also possible to discern a certain low frequency modulation at the Ball Pass Frequency (*BPF*) due to the bearing variable compliance. In practice the presence of this modulation will be difficult to identify, in part due to the use preloads to remove the bearing clearance but also because of the sliding of rolling elements instead of pure rolling assumed in the formulation. When torque is increased, the average *LTE* is shifted to the lower part of the figure increasing their absolute amplitude. This is because bearing and shaft deflections lead to increments in the effective gear centre distance. Thus, the starting and ending time of contact between successive pairs of teeth becomes modified and therefore the shape of the *LTE* time record.

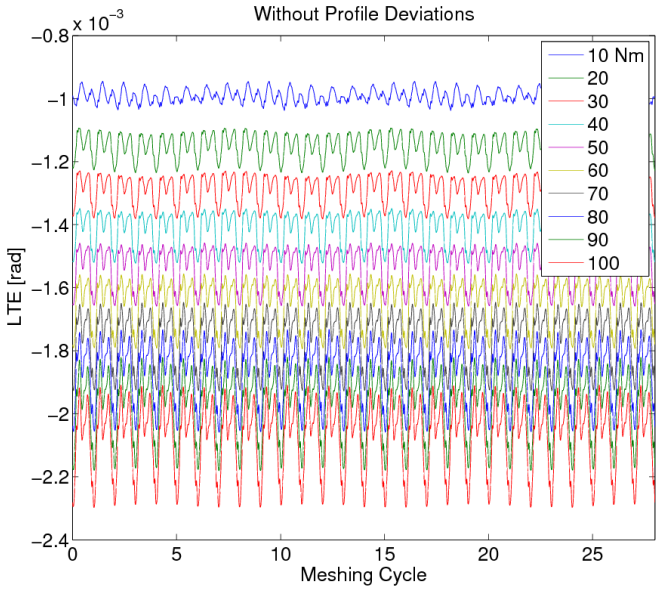

Figure 13.- Dynamic *LTE* without profile deviation at 1000 rpm for several torques

The increment on the centre distances can be seen in Figure 14 where the orbits for each gear centre are presented. There, the dashed line represents the bearing clearance. In contrast with the quasi-static results in Figure 5, dynamic terms in the equation system (2) increase the amplitude of displacements along the *LOA*. Meanwhile, the amplitude of the orbit in the OLOA as a function of the applied torque follows a similar pattern to that obtained in quasi-static analysis with narrower amplitudes for minimum and maximum torque values (see Figure 7).

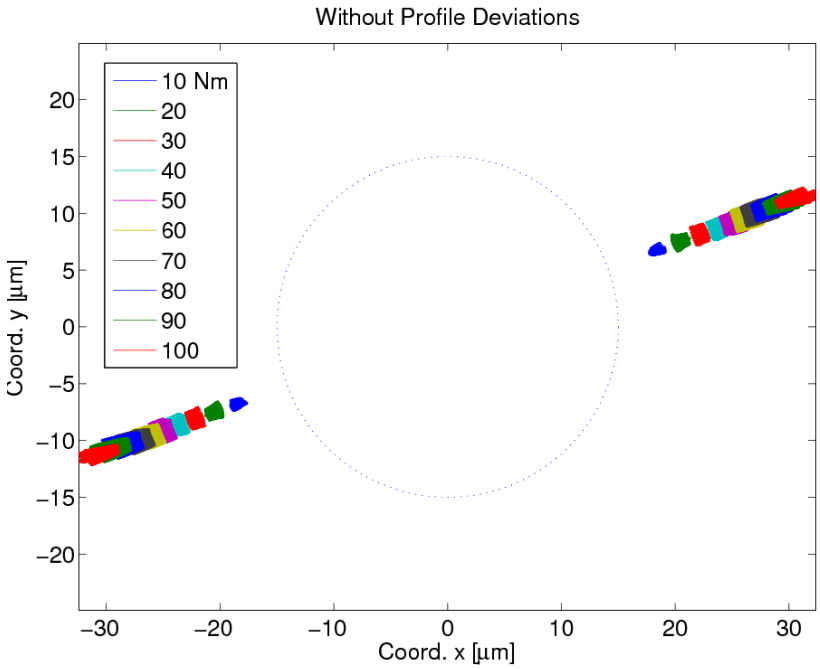

Figure 14.- Gear center orbits without profile deviations at 1000 rpm for several torques. Dashed line represents bearing clearance.

Gear transmissions are usually monitored by accelerometers disposed in the case, near to the bearing supports, with their main axis parallel to the *LOA*. Thus, the forces transmitted by the bearings are of main interest. With this aim, the changes on the pressure angle due to the variation in the gear center distance were neglected and the bearing forces on the *LOA* are derived from their x and y components. The spectrum corresponding to the force obtained at bearing 1b1 (see Figure 1) is presented in Figure 15. As expected, the spectrum is dominated by the harmonics of the Gear Mesh Frequency (*GMF*). Moreover, it could be appreciated *GMF* sidebands corresponding to the modulation due to the ball pass frequency. The latter is also present in the zone of low frequencies where it can be seen up to three *BPF* harmonics. Again, in practice, noise and the sliding of rolling elements instead of the pure roll assumption made in the bearing model attenuate this phenomenon, so that the spectra usually do not exhibit these frequencies. Furthermore the *GMF* modulation in real cases is even more complex, being basically determined by the eccentricities and pitch errors which are not considered in this work, so that the side bands appear at distances matched to integer multiples of the frequency of shaft.

The relationship between the value of the transmitted torque and the amplitude of the *GMF* harmonics is not clear although in general it seems that the latter increases when torque is higher. Nevertheless, the rising of the *GMF* amplitude with the torque is not linear and each harmonic follows a different path. The most important change lies on the amplitude of the 5^{th} *GMF* harmonic that undergoes a clear growth becoming dominant when the loads are higher, whereas for low torques it is the 2^{th} one.

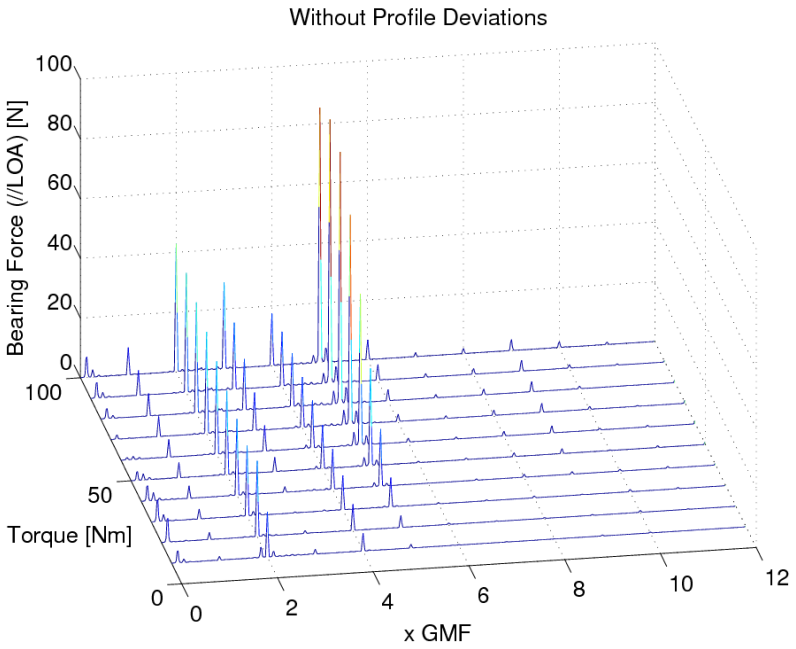

Figure 15.- Spectrum of the transmitted force in the *LOA* on the so-called bearing b_{11} without profile deviations at 1000 rpm for several torques.

5.2. Dynamics simulations with *PE*

The *PE* described in previous section has been added to the dynamic simulations obtaining the *LTE* shown in Figure 16. In contrast with the results obtained in absence of *PE*, the peak to peak amplitude is clearly higher and this fact is more noticeable for low torque values. That is consistent with the results obtained in the quasi-static analysis, where torque increments imply a reduction of differences with respect to the model without *PE* (see Figure 7).

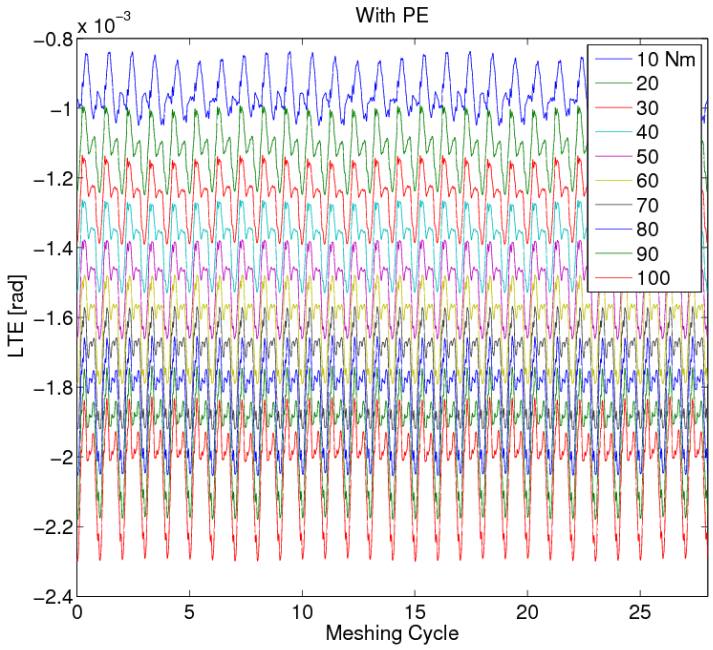

Figure 16.- Dynamic *LTE* with *PE* at 1000 rpm for several torques.

Regarding gear centre orbits, *PE* induce a slight enlargement in the *LOA* direction with respect to the model without profile error, particularly with low torques, as can be seen in Figure 17.

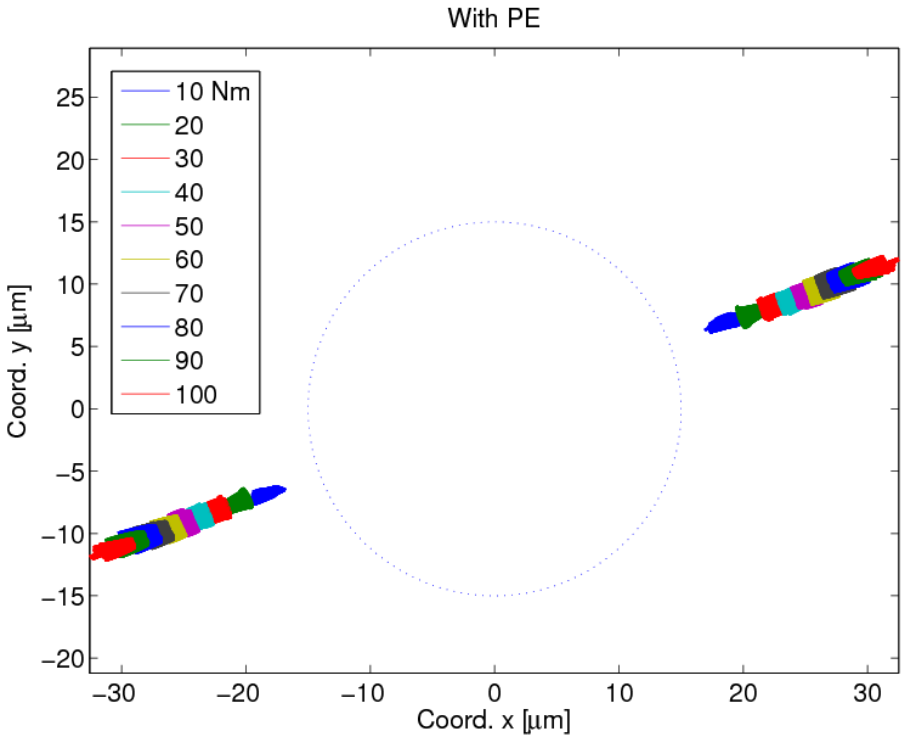

Figure 17.- Gear center orbits with *PE* at 1000 rpm for several torques. Dashed line represents bearing clearance.

In Figure 18 the spectrum corresponding to the transmitted force on bearing b_{11} parallel to the *LOA* is presented. Some differences can be appreciated for the amplitude of the 4^{th} GMF harmonic which is clearly higher for all the torque values analysed when *PE* are included in the simulation. On the other side, *PE* increases the 3th GMF amplitude for low torque values whereas reduce it for higher transmitted torque. However the spectrum obtained with and without *PE* for a certain torque presents a similar pattern with little differences in certain harmonics more noticeable for low torque. Nevertheless, in general, *PE* tends to increase the amplitude of GMF harmonics, fact consistent with experimental observations which report lower noise levels when more accurate gears are used.

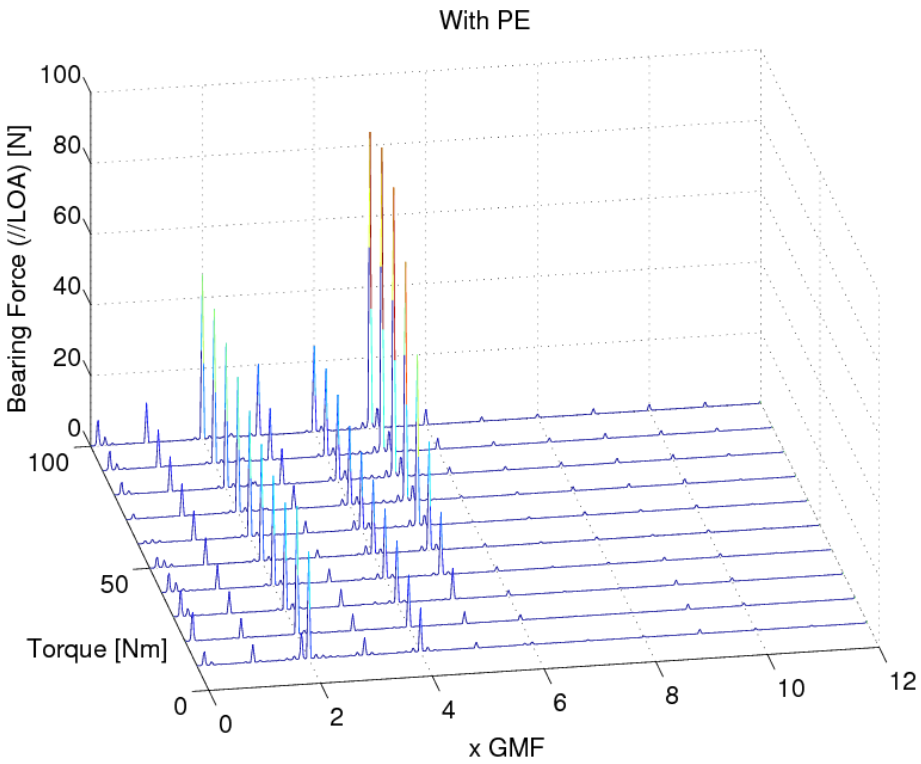

Figure 18.- Spectrum of the transmitted force in the *LOA* on the so-called bearing b_{11} with *PE* at 1000 rpm for several torques.

5.3. Dynamics simulations with *Tip Relief*

Regarding profile relief, only the case *TRL4C015* was considered (see Table). This relief was included in both gears providing a design load close to 30 Nm (see Figure 8) and showing notable changes as a function of the transmitted torque. Figure 19 presents the *LTE* obtained in dynamic simulations. As expected, the inclusion of tip relief results in a clear reduction when the transmission works close to the design load although this time this seems to be located near 40 Nm. The difference perhaps lies on the changes in the gear centre distance included in the dynamic simulations and not considered in the quasi-static analysis presented in section 5.

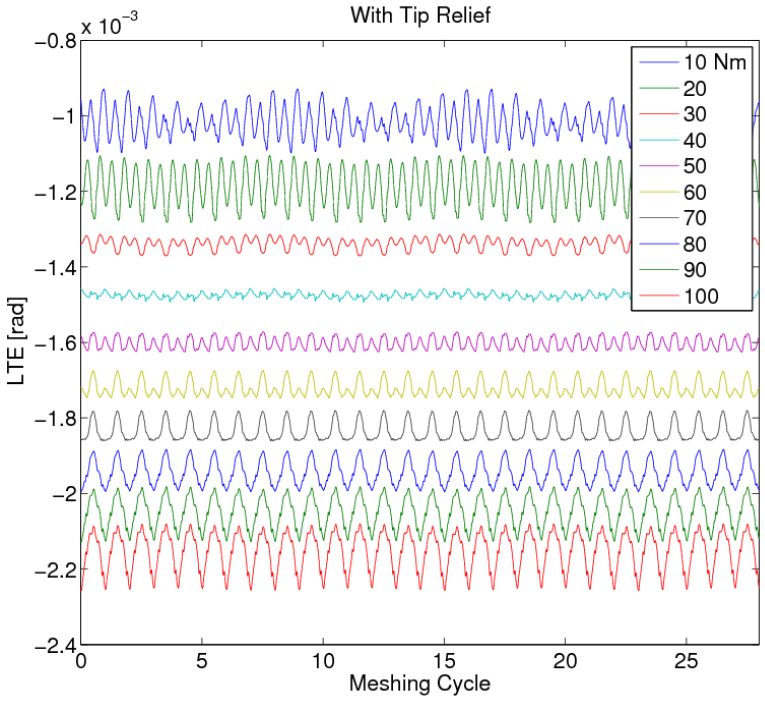

Figure 19.- Dynamic *LTE* with Tip Relief (*TRL4C015*) at 1000 rpm for several torques This reduced *LTE* leads to more contained orbits in the *LOA* direction with respect the orbits obtained without profile deviations except for low torque values (10 and 20 Nm) as can be observed in Figure 20.

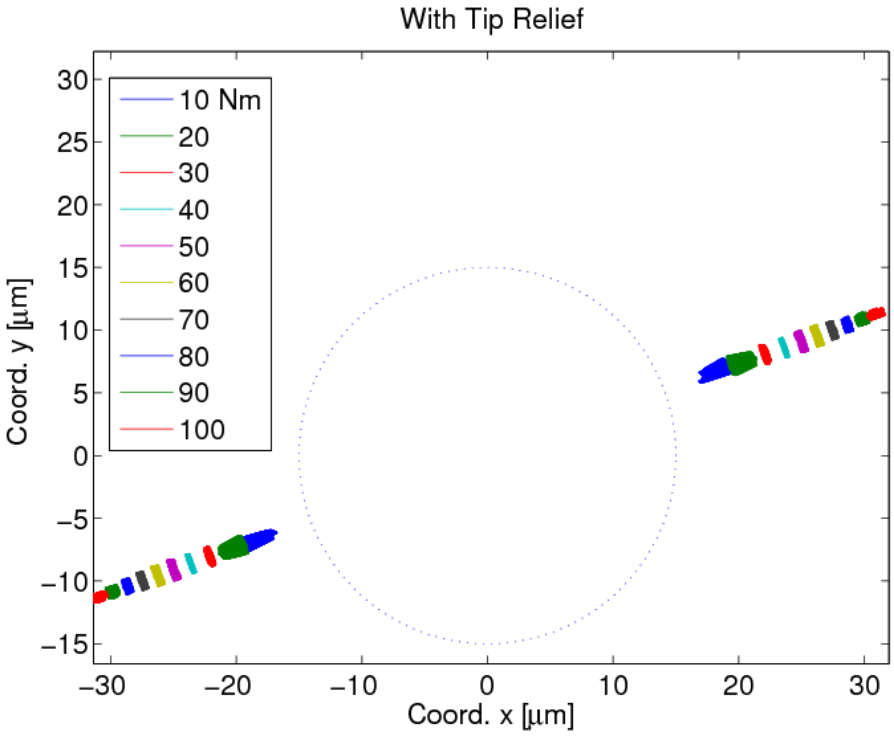

Figure 20.- Gear center orbits with Tip Relief (*TRL4C015*) at 1000 rpm for several torques. Dashed line represents bearing clearance.

Moreover, tip relief provides lower amplitude for the harmonics of the forces transmitted to the supports (see Figure 21), regardless of the level of load applied, although this reduction is more significant in the vicinity of the design load. Thus, as expected, the dynamic behaviour of the gear transmission is greatly improved for torque loads close to the design load, but also produces a significant reduction in amplitude of the harmonics of the GMF when the torque levels are higher.
It is particularly remarkable the reduction of the magnitude of the 5th GMF harmonic, even though it remains the dominant one when the torque is high. By contrast, the tip relief analysed highlights the magnitude of the 2nd GMF harmonic when low torques are considered (10 to 20 Nm).

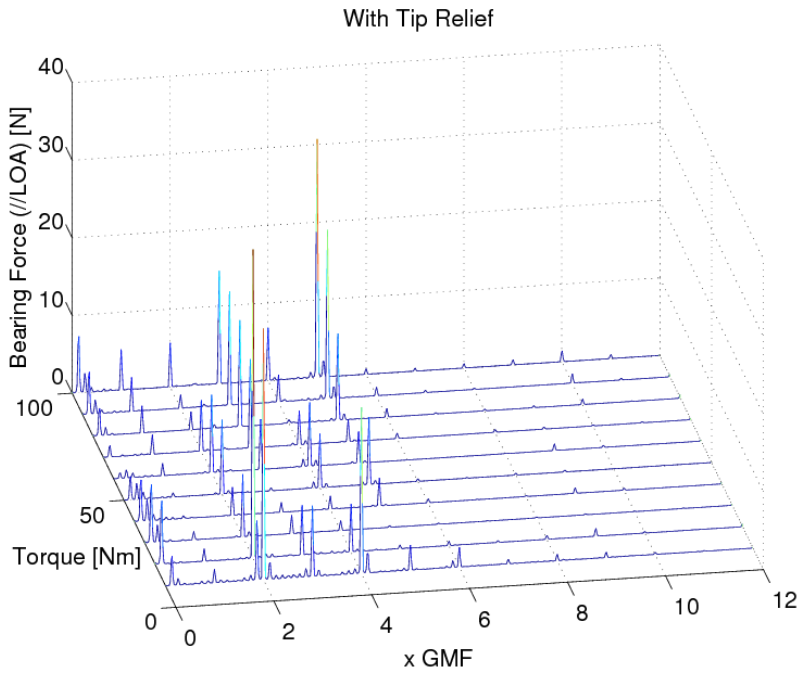

Figure 21.- Spectrum of the transmitted force in the *LOA* on the so-called bearing b_{11} with Tip Relief (*TRL4C015*) at 1000 rpm for several torques.

5 Conclusions

A non-linear model for the dynamic analysis of a gear transmission supported by ball bearings which includes tooth profile deviations has been presented. The model approach used for the calculation of meshing forces, which combines *FE* analysis and analytical formulation, enables a very straightforward implementation of the tooth profile deviations. The model's effectiveness is shown by means of an application example which assesses the consequences when deviations are introduced, with particular attention to the role played by the torque level. The tip relief cases analysed show a generalized enhancement of the *LTE* values and gear centre orbit amplitudes, with much less improvement for low values of torque. Regarding *PE*, the model is also

capable of predicting the increase of the *LTE* amplitude and orbits along the *LOA*, showing a much greater effect for low torques. In addition, the model is also able to explain the bearing clearance and variable stiffness effect on the *LTE* results widening the orbits *OLOA*.

6 Acknowledgements

This paper has been developed in the framework of Project DPI2006-14348 funded by the Spanish Ministry of Science and Technology.

7 References

[1] P. Velex, M. Maatar, A mathematical model for analyzing the influence of shape deviations and mounting errors on gear dynamic behaviour, J .Sound Vibrat., 191 (1996) 629-660.
[2] F. Viadero, A. Fernandez Del Rincon, R. Sancibrian, P. Garcia Fernandez, A. De Juan, A model of spur gears supported by ball bearings, WIT Transactions on Modelling and Simulation 46 (2007) 711-722.
[3] A. Fernandez del Rincon, F. Viadero, R. Sancibrian, P. Garcia Fernandez, A. De Juan, A dynamic model for the study of gear transmissions, WIT Transactions on Modelling and Simulation 48 (2009) 523-534.
[4] A.F. Del Rincon, F.V. Rueda, M.I. Santamaria, P.G. Fernandez, A. De-Juan De Luna, R.S. Herrera, Load effects on the dynamics of spur gear transmissions, ASME 2010 10th Biennial Conference on Engineering Systems Design and Analysis, ESDA2010 5 (2010) 369-378.
[5] Fernandez Del Rincon A, Iglesias M, De Juan A, Viadero F. Defect simulation in a spur gear transmission model. New Trends in Mechanism Science: Analysis and Design, Mechanisms and Machine Science 5: Springer; 2010. p. 191-198.
[6] A. Kahraman, R. Singh, Non-linear dynamics of a spur gear pair, J .Sound Vibrat ., 142 (1990) 49-75.
[7] G. Bonori, F. Pellicano, Non-smooth dynamics of spur gears with manufacturing errors, J .Sound Vibrat ., 306 (2007) 271-283.
[8] J.R. Ottewill, S.A. Neild, R.E. Wilson, An investigation into the effect of tooth profile errors on gear rattle, J .Sound Vibrat ., 329 (2010) 3495-3506.
[9] J. Shengxiang, H. Ian, W. Jiande, The Dynamic Modeling of Multiple Pairs of Spur Gears in Mesh, Including Friction and Geometrical Errors, International Journal of Rotating Machinery 9 (2003) 437-442.
[10] L. Vedmar, A. Andersson, A method to determine dynamic loads on spur gear teeth and on bearings, J .Sound Vibrat ., 267 (2003) 1065-1084.
[11] F.L. Litvin, A. Fuentes, Gear geometry and applied theory, 2nd ed., Cambridge,2004.
[12] S. Fukata, E.H. Gad, T. Kondou, T. Ayabe, H. Tamura, on the radial vibration of ball bearings. (Computer simulation). 28 (1985) 899-904.
[13] E. Mucchi, G. Dalpiaz, A. Rivola, Elastodynamics analysis of a gear pump. Part II: Meshing phenomena and simulation results, Mechanical Systems and Signal Processing, 24 (2010), 2180 – 2197.
[14] American National Standard,Accuracy Classification System – Tangential Measurements for Cylindrical Gears (2002).
[15] T. Harris, M. Kotzalas, Rolling Bearing Analysis, John Wiley & Sons Inc,2001.
[16] S. He, R. Gunda, R. Singh, Effect of sliding friction on the dynamics of spur gear pair with realistic time-varying stiffness, J. Sound Vibrat., 301 (2007) 927-949.
[17] G. Bonori, F. Pellicano, Non-smooth dynamics of spur gears with manufacturing errors, J. Sound Vibrat. 306 (2007), 271-283.
[18] A. Fernández del Rincón, F. Viadero, M. Iglesias, P. García, A. de-Juan, R. Sancibrián, A model for the study of meshing stiffness in spur gear transmissions, Mechanism and Machine Theory, 61 (2013), 30-58.